Modern Physics Letters B, Vol. 17, No. 17 (2003) 941–948

World Scientific
www.worldscientific.com

REGULARITY–PARTIAL CHAOS–REGULARITY TRANSITION AND OVERLAPPED KAM SCENARIOS IN A CONSERVATIVE SYSTEM OF TWO LINEARLY COUPLED DOUBLE-WELL OSCILLATORS

V. PAAR* and N. PAVIN

Department of Physics, Faculty of Science, University of Zagreb,
10000 Zagreb, Croatia
**paar@hazu.hr*

Received 14 May 2003

For linearly coupled double-well oscillators the regularity–partial chaos–regularity transition is found. First, an incomplete KAM scenario develops with increasing energy, from integrable pattern comprising in-phase and out-of-phase small elliptic orbits towards a partial chaos, with a deformed regular island immersed in a chaotic sea. At a critical energy a new deformed island appears as a mirror image. Above the critical energy the inverse KAM scenario leads to gradual destruction of partial chaos and to the appearance of large elliptic orbits which correspond to the large-amplitude limit governed by uncoupled oscillators with cubic anharmonicities.

Keywords: Double-well oscillator; coupled oscillators; KAM; chaos; chaos–regularity transition; Poincare section; conservative system.

PACS Number(s): 05.45.+b

1. Introduction

In the famous Henon–Heiles model[1–5] two single-well oscillators, one harmonic and another nonlinear, are coupled by a cubic interaction term in the Hamiltonian with both the coupling and anharmonicity parameters having constant values. Therefore, the extent of destruction of KAM tori and of the onset of chaos in the framework of the general Kolmogorov–Arnold–Moser (KAM) theorem[6] depends only on energy. As the energy increases, the KAM tori gradually dissolve and the chaotic regions gradually expand with increasing energy. Finally, after the last KAM torus has disappeared at sufficiently high energy, a single chaotic trajectory covers the entire allowed region of phase space. Such behavior is considered as a scenario for the universal behavior of nonintegrable Hamiltonian systems.[7,8]

Chaotic patterns have also been studied for two single-well oscillators coupled by a symmetric quartic interaction term in the Hamiltonian.[9,10,11,12] Investigations of the energy dependence of Poincare sections at fixed parameter values have led to similar conclusions as in the case of the Henon–Heiles system, i.e. that the behavior

changes with increasing energy from regular to chaotic.[9,10]

A more complex pattern was obtained in the investigations of the double pendulum with the regularity–chaos–regularity transition.[11] Another type of complex pattern was found to have a dependence on the varying of the coupling parameter between two nonlinearly coupled oscillators, with transition from chaos to regularity and again to chaos so that the behavior of the system is not simply divided by a single critical coupling parameter into a regular and chaotic region, but is divided by two critical coupling parameters into two chaotic regions separated by a regular region.[12]

2. Nonlinear System of Two Linearly Coupled Double-Well Oscillators

In this paper we study the energy dependence of regular and chaotic pattern in a model of two linearly coupled double-well oscillators. This system is governed by the equations of motion:

$$\begin{aligned} \ddot{x} - x + x^3 + \alpha(x - y) &= 0\,, \\ \ddot{y} - y + y^3 + \alpha(y - x) &= 0\,, \end{aligned} \tag{1}$$

where α is the coupling parameter.

We note that a double-well oscillator with external forcing (Duffing oscillator) has been previously investigated in many studies.[13–19] On the other hand, the appearance of linear coupling between two oscillators in the equations of motion was pointed out in connection with scalar diffusion[20] and with the nonlinear mass-spring system.[21]

For a fixed value of coupling parameter α and of energy E the system (1) is described using the $(x, \dot{x})$ Poincare sections defined by the $y = 1, \dot{y} > 0$ plane in four-dimensional phase space. To fill out the Poincare section a set of initial conditions extended over the energetically accessible region are chosen.

For $\alpha = 0$ the two oscillators, denoted as the x-oscillator and y-oscillator, are decoupled and the system (1) is integrable. Each oscillator has two stable equilibrium points at the positions -1 and 1, and the saddle point at the position 0. By coupling the x- and y-oscillators, i.e. for $\alpha \neq 0$, the wells of each oscillator become asymmetric and already for weak coupling, $\alpha \leq 0.01$, chaotic behavior extends over some noticeable regions of phase space. In this case the potential energy surface for the system (1) (Fig. 1) has four stable equilibrium points, at the positions $(x, y) = (-1, -1)$, $(-\sqrt{1-2\alpha}, \sqrt{1-2\alpha})$, $(\sqrt{1-2\alpha}, -\sqrt{1-2\alpha})$ and $(1, 1)$, forming a quadrangle. Four saddle points are situated at $(x, y) = (a, -b), (-a, b), (b, -a), (-b, a)$, where $a = \sqrt{(1-\alpha+\sqrt{1-2\alpha-3\alpha^2})/2} \approx 1-\alpha$, $b = \sqrt{(1-\alpha-\sqrt{1-2\alpha-3\alpha^2})/2} \approx \alpha$, and one unstable equilibrium point is placed at the origin $(x, y) = (0, 0)$. The coupling between x- and y-oscillators introduces asymmetry in the wells for the choice of the Poincare plane $y = 1$ so that the depth of left well of the x-oscillator becomes $1/2 - 2\alpha + 2\alpha^2$, i.e. smaller than the depth $1/2$ of the right well.

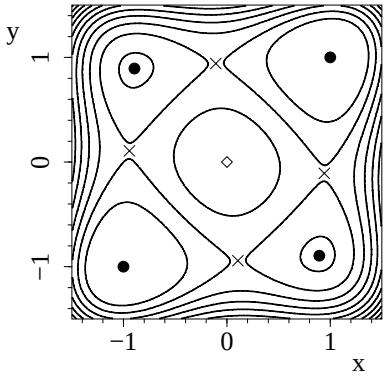

Fig. 1. Potential energy surface associated with the system (1) at $\alpha = 0.1$. The positions of stable equilibrium points (•), unstable equilibrium point (◇) and saddles (×) are shown.

At a fixed value of energy, the fraction of chaotic regions in the Poincare section gradually increases with increasing coupling strength α.

The aim of the present investigation is to study how the fraction of chaotic regions evolves with increasing energy at a fixed coupling strength. In Fig. 2 we display some characteristic Poincare sections with increasing energy for the coupling parameter $\alpha = 0.1$. The Poincare sections calculated for the system (1) can be classified as follows.

2.1. *KAM scenario at low energy*

At low energies, between the bottoms of two potential wells of the x-oscillator, the Poincare section exhibits an integrable pattern (Fig. 2(a)). The orbits are trapped in the right well. (An orbit trapped in one of the two potential wells is referred to as a small orbit.) The Poincare section has two elliptic points on the $\dot{x}$-axis, one with $\dot{x} > 0$ and the other with $\dot{x} < 0$, representing two periodic trajectories. In the first case, the x-oscillator and y-oscillator are in phase and in the second they are out of phase. Each elliptic point is surrounded by a family of elliptic orbits, representing quasiperiodic trajectories. These two families of orbits will be referred to as the in-phase family and out-of-phase family, respectively. We note that a similar pattern of Poincare section at low energy has been previously obtained in several cases: for an integrable two-dimensional potential with anharmonicities up to the fourth order terms,[22] for a double pendulum at low energy[11] and for two-dimensional subspace of a five-dimensional nonlinear oscillator at low energy.[23]

This type of Poincare sections arises also by linearizing the equations of motion (1), which results in an integrable system of two linearly coupled harmonic oscillators:

$$\begin{aligned} \ddot{x} - x + \alpha(x - y) &= 0\,, \\ \ddot{y} - y + \alpha(y - x) &= 0\,. \end{aligned} \tag{2}$$

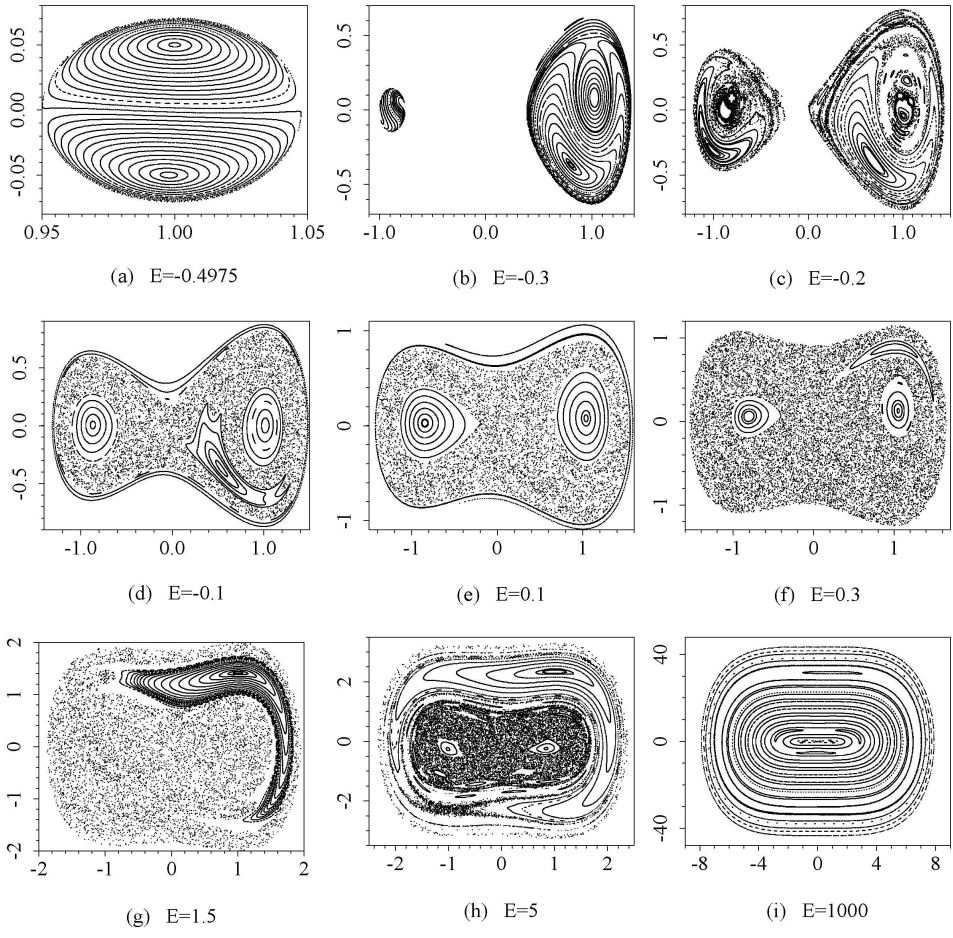

Fig. 2. Poincare sections $(x, \dot{x})$ of the system (1) at the coupling strength $\alpha = 0.1$ for increasing values of energy E: (a) -0.4975, (b) -0.3, (c) -0.2, (d) -0.1, (e) 0.1, (f) 0.3, (g) 1.5, (h) 5 and (i) 1000.

Introducing $u = x + y$, $z = x - y$ the equations in (2) are transformed into two uncoupled harmonic oscillators, with frequencies $\omega_1 = 1$ and $\omega_2 = \sqrt{1 + 2\alpha}$. Let us consider solutions $u = A\cos(\omega_1 t - \phi_1)$, $z = B\cos(\omega_2 t - \phi_2)$, where we take $\phi_1 = \phi_2 = 0$, and A, $B > 0$.

For $z = 0$, i.e. $B = 0$, the amplitude A has the maximum value A_m corresponding to the energy E. Then

$$y = x = \frac{1}{2} A_m \cos\omega_1 t, \qquad \dot{y} = \dot{x} = -\frac{1}{2} A_m \omega_1 \sin\omega_1 t\,. \tag{3}$$

In this case the Poincare plane is defined by the position of the potential well $y = 0$, and $\dot{y} > 0$. From $y = \frac{1}{2} A_m \cos\omega_1 t = 0$ we have $\omega_1 t = \pi/2,\ 3\pi/2,\ 5\pi/2,\ 7\pi/2,\ \ldots$

but only the values

$$\omega_1 t = \frac{3\pi}{2}, \frac{7\pi}{2}, \ldots \tag{4}$$

satisfy the condition $\dot{y} = -\frac{1}{2} A_m \omega_1 \sin \omega_1 t > 0$. For the $\omega_1 t$ values (4) we obtain from (3):

$$x(\omega_1 t) = 0, \qquad \dot{x}(\omega_1 t) = \frac{A_m \omega_1}{2} = \frac{A_m}{2}\,.$$

This periodic orbit corresponds to the upper elliptic point in Fig. 2(a).

In a similar way, for $u = 0$, i.e. $y = -x$ we obtain the periodic orbit:

$$x(\omega_2 t) = 0, \qquad \dot{x}(\omega_2 t) = -\frac{B_m \omega_2}{2} = -\frac{B_m \sqrt{1+2\alpha}}{2}\,,$$

which corresponds to the lower elliptic point in Fig. 2(a).

For increasing values of energy the energetically accessible phase space region increases, but the two families of elliptic orbits trapped in the right potential well behave differently. The region covered by the out-of phase (lower) family of elliptic orbits grows faster than the region of the in-phase (upper) family of elliptic orbits, which is being encircled by the out-of phase elliptic orbits (Fig. 2(b)). The out-of-phase elliptic point is being shifted to the left and its elliptic orbits become more and more deformed. Furthermore, an additional elliptic point appears above the in-phase elliptic point. Its elliptic orbits are squeezed into a narrow strip. With increasing energy, quasiperiodic orbits also appear in the left potential well, as it becomes energetically accessible (Fig. 2(b)).

Increasing the energy further, the KAM scenario develops for orbits trapped within the right and within the left potential well (Fig. 2(c)) and the first patches of chaotic regions are noticeable. With a further increase of energy the orbits moving through both potential wells, referred to as large orbits, become energetically accessible. This is accompanied by a rapid onset of chaos, so that about 60% of the available phase space is covered by chaotic orbits, and the remaining KAM tori are restricted to three main islands, two trapped in the right potential well and one in the left (Fig. 2(d)). In the region of the right potential well there is a central island of elliptic orbits (originating from the in-phase family of quasiperiodic orbits of the low-energy integrable case) and below to the left is a deformed island (originating from out-of-phase family of the low-energy integrable case). In the region of the left potential well only the central island is pronounced. There are also some narrow strips of large elliptic orbits encircling the chaotic sea.

2.2. *Overlapped KAM and inverse KAM scenarios at intermediate energies*

With a further increase in energy the KAM tori in the deformed island are fully destroyed and two islands at the positions of two potential wells are the only pronounced regular regions immersed into the chaotic sea (Fig. 2(e)). Up to this point

the pattern of the onset of chaos is in accordance with expectations based on the universal behavior of nonintegrable Hamiltonian systems.[7,8]

We note that, as expected, the causes of chaotic behavior are homoclinic orbits connecting stable and unstable manifolds of saddle points. For the case of Fig. 2(e) these manifolds are calculated by taking initial conditions in a small circular disc of radius 0.015 surrounding the most pronounced saddle point $(0.516, -0.355)$ and following the evolution of the system in forward and in backward directions of time (Fig. 3).

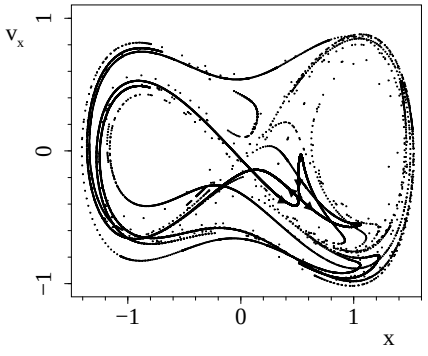

Fig. 3. Poincare section for stable and unstable manifolds calculated for a saddle point in the case of Fig. 2(e).

With a further increase in energy the two islands continue to decrease in size, but an additional deformed island appears above the position of the left island (Fig. 2(f)). This deformed island qualitatively corresponds to a mirror image of deformed island from Fig. 1(d) with respect to the x-axis.

As the energy increases further, the two islands situated at the positions of the two wells gradually shrink, but contrary to expectations the newly born deformed island increases in size (Fig. 2(f)). Finally, the two islands disappear while the new deformed island grows in size (Fig. 2(g)).

2.3. *Inverse KAM scenario at high energies*

As the energy is increased further, an inverse KAM scenario developes. The chaotic sea gradually shrinks and the two islands reappear at the positions of the two wells, accompanied by more and more surrounding island chains and elliptic orbits (Fig. 2(h)). Simultaneously, the outer deformed orbit continues to grow and encircles the shrinking region of the chaotic sea.

Finally, as the energy increases further, chaotic regions gradually dissolve and the system approaches the regular pattern (Fig. 2(i)). This structure is dominated by a family of large elliptic orbits. Within this set of large orbits lies a system of small elliptic orbits within each of the two potential wells and some encircling island

chains, barely visible in the figure. Close to the upper boundary of the energetically accessible region there is a deformed island of elliptic orbits, squeezed between the large orbits, as a remnant of the deformed island from Fig. 2(h). In the limit of very large energy, the pattern of Poincare section asymptotes to the set of large elliptic orbits, which corresponds to the limit of integrable system:

$$\begin{aligned} \ddot{x} + x^3 &= 0\,, \\ \ddot{y} + y^3 &= 0\,, \end{aligned} \tag{5}$$

which arises from (1) in the large amplitude limit $x,\, y \gg 1$.

We note a particular role of the upper deformed island in bridging the pattern of the KAM scenario up to the critical energy of ≈ 0.5 and of the inverse KAM scenario above that energy. This is different from the results of previous investigations of the change of pattern between the integrable limits at low and high energy for double pendulum, where the KAM scenario leads to a fully ergodic motion.[11]

3. Conclusion

A summary of the behavior of the system (1) is presented in the graph of Fig. 4, displaying the calculated chaotic fraction of energetically available phase space in Poincare sections with dependence on energy. In accordance with Fig. 1 the fraction of the chaotic surface first grows with increasing energy up to the energy of ≈ 0.5, reaching a maximum value of 93%. With a further increase in energy this fraction gradually decreases, but at a lower rate. The increase in chaotic fraction from the lowest energy -0.5 to the critical energy of 0.5 is not monotonic. There is a pronounced drop in the chaotic fraction at the energy $E = 0$, at which the central unstable equilibrium point $(x,\, y) = (0,\, 0)$ is reached, so that large orbits become energetically accessible.

Concluding, conservative systems of two coupled nonlinear oscillators can exhibit different types of chaotic behavior with increasing energy, depending on

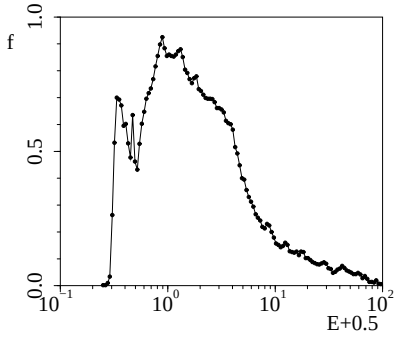

Fig. 4. Chaotic fraction of the energetically accessible region in the Poincare section with dependence on energy for the system (1). For each value of energy the chaotic fraction is calculated by using a grid with 500 initial positions.

anharmonicities and coupling. For the Henon–Heiles system and for a system with quartic coupling in the Hamiltonian, a standard situation of the full KAM scenario is developed with increasing energy, leading to regular and then chaotic motion.[1,2,9,10] On the other hand, for the two linearly coupled nonlinear oscillators investigated here, starting from an integrable case the KAM scenario develops with energy up to a certain point, but a fully developed chaos is not reached. Above the critical energy an inverse KAM scenario leads to transition back to an another integrable case.

References

1. H. Henon and C. Heiles, *Astrophys. J.* **69**, 73 (1964).
2. M. Henon, in *Chaotic Behavior of Deterministic Systems*, eds. G. Iooss, R. H. G. Helleman and R. Stora (North-Holland, Amsterdam, 1983), p. 53.
3. P. Finkler, C. E. Jones and G. A. Sowell, *Phys. Rev.* **A44**, 925 (1991).
4. S. Udry and L. Martinet, *Physica* **D44**, 61 (1990).
5. P. Cipriani and M. Di Bari, *Phys. Rev. Lett.* **81**, 5532 (1998).
6. V. I. Arnol'd, *Mathematical Methods in Classical Mechanics* (Springer, New York, 1978).
7. R. C. Hilborn, *Chaos and Nonlinear Dynamics* (Oxford University Press, New York, 1994).
8. E. Ott, *Chaos in Dynamical Systems* (Cambridge University Press, Cambridge, England, 1993).
9. L. A. Bunimovich, *Commun. Math. Phys.* **65**, 295 (1979).
10. R. Z. Sagdeev, D. A. Usikov and G. M. Zaslavsky, *Nonlinear Physics* (Harwood Academic Publishers, Chur, 1992).
11. H. J. Korsch and H. J. Jodl, *Chaos* (Springer-Verlag, Berlin, 1994).
12. Z. Deng and F. T. Hioe, *Phys. Rev. Lett.* **55**, 1539 (1985).
13. P. Holmes, *Phil. Trans. Roy. Soc.* **A292**, 419 (1979).
14. F. C. Moon, *ASME J. Appl. Mech.* **47**, 638 (1980).
15. Y. H. Kao, J. C. Huang and Y. S. Gou, *Phys. Rev.* **A35**, 5228 (1987).
16. F. T. Arecchi, R. Badii and A. Politi, *Phys. Rev.* **A32**, 402 (1985).
17. P. Holmes and D. Whitley, *Physica* **D7**, 111 (1983).
18. F. C. Moon, *Phys. Rev. Lett.* **53**, 962 (1984).
19. V. English, *Phys. Rev.* **A44**, 916 (1991).
20. R. Ermentrout, in *Nonlinear Oscillations in Biology and Chemistry*, ed. H. G. Othmer (Springer-Verlag, Berlin, 1980), p. 98.
21. R. M. Rosenberg, *Adv. Appl. Mech.* **9**, 155 (1966).
22. P. W. Cleary, *Phys. Rev.* **A41**, 2924 (1990).
23. V. Paar, D. Vorkapić and A. E. L. Dieperink, *Phys. Rev. Lett.* **69**, 2184 (1992).